1 February 2001

ELSEVIER

Optics Communications 188 (2001) 69–76

OPTICS COMMUNICATIONS

www.elsevier.com/locate/optcom

Photorefractive steady state solitons up to telecommunication wavelengths in planar SBN waveguides

M. Wesner [a,*], C. Herden [a], D. Kip [a], E. Krätzig [a], P. Moretti [b]

[a] *Fachbereich Physik, Universität Osnabrück, 49069 Osnabrück, Germany*

[b] *Laboratoire de Physico-Chimie des Matériaux Luminescents, Université Claude Bernard Lyon1, 69622 Villeurbanne, France*

Received 1 August 2000; received in revised form 2 November 2000; accepted 4 December 2000

Abstract

We experimentally demonstrate strong photorefractive self-focusing and soliton formation in Rh-doped strontium–barium niobate waveguides at telecommunication wavelengths up to $\lambda = 1.5$ μm. A comparison of soliton formation at different wavelengths in the visible and infrared region is carried out. We measure the electrooptic coefficient r_{33}, analyze the soliton width, the accessible intensity range, and the wavelength dependence of the so-called 'dark intensity'. © 2001 Elsevier Science B.V. All rights reserved.

PACS: 42.65; 42.79; 78.20

Keywords: Photorefractive materials; Spatial solitons; Nonlinear optics; Nonlinear waveguides

1. Introduction

Self-trapping of light beams in ferroelectric oxide crystals has been intensively investigated since the first prediction of photorefractive solitons in 1992 [1]. In particular, soliton formation was observed in $Sr_{1-x}Ba_xNb_2O_3$ (SBN) [2], $KNbO_3$ [3], and $Bi_{12}TiO_{20}$ [4]. In these crystals, the photorefractive effect can lead to the self-focusing of a light beam. If the natural diffraction of the light is exactly balanced by the self-focusing, a spatial soliton is formed.

Photorefractive solitons possess favorable properties in forming and steering light beams and therefore are often proposed for applications in all-optical signal processing [5,6]. For this purpose, the soliton properties around the telecommunication wavelengths of 1.3 and 1.5 μm need to be investigated. However, up to now, photorefractive solitons at these wavelengths have only been observed in semiconductors like InP:Fe [7]. In ferroelectric crystals, the photorefractive effect usually requires visible light to excite charge carriers from impurity levels in the broad band gap. Therefore, in the past, investigations of self-trapping phenomena have been concentrated on this wavelength region. Concerning telecommunication applications, it was suggested to induce solitons with visible light and to guide intense infrared beams in the induced channels [5,8]. This, however, is only practicable if the infrared beam itself has no influence on the photorefractive process.

* Corresponding author. Fax: +49-541-969-3510.

E-mail address: motte@sedan.uni-osnabrueck.de (M. Wesner).

PII: S0030-4018(00)01160-3

Refractive index changes which can be induced by infrared light are often small and do not cause noticeable effects. To our knowledge there is only one publication dealing with a photorefractive one-photon process at telecommunication wavelengths [9] in an oxide crystal: Two-beam coupling is demonstrated up to $\lambda = 1.5$ μm in a high-dose ion-implanted $KNbO_3$ waveguide. Efficiency and build-up speed of the holographic gratings are shown to decrease considerably with increasing wavelength. However, we will demonstrate here that soliton formation is possible even with small refractive index changes achievable in the infrared. This can be understood in the following way: A soliton can be regarded as a light beam that induces its own waveguide [10]. For guided modes it is well known that any small localized refractive index change can guide a wave, if the corresponding mode is broad enough. Spatial solitons are formed just like this: the soliton becomes broader with increasing wavelength due to the smaller refractive index change, but nevertheless a stable soliton can be created.

In this contribution we investigate self-focusing and soliton formation at telecommunication wavelengths using a planar SBN waveguide. We demonstrate that focusing strengths and build-up times of the same magnitude as in the visible wavelength region are possible. A comparison of soliton formation at different wavelengths in the visible and infrared is provided.

2. Theoretical background

The photorefractive effect is induced by an inhomogeneous intensity distribution, for instance a single Gaussian beam. In ferroelectric oxide crystals the illumination produces charge carriers which are then redistributed. The dominating charge transport mechanism responsible for self-focusing and soliton formation is drift in an external electric field [11]. The diffusion mechanism mainly causes a lateral bending of the beam and is neglected in this investigation [12]. After drift-induced redistribution, retrapped charges build up a space charge field E_{sc} which changes the refractive index via the electrooptic effect,

$$\Delta n = -\tfrac{1}{2} n_e^3 r_{33} E_{sc}. \tag{1}$$

Here n_e denotes the extraordinary refractive index and r_{33} is the element of the electrooptic tensor according to our experimental geometry. The space charge field E_{sc} for self-focusing can be written as [13]

$$E_{sc} = E_{ext} \frac{I_d}{I_d + I_b(x)} = E_{ext} \frac{1}{1 + I_b(x)s/\beta}, \tag{2}$$

with $I_d := \beta/s$. Here $I_b(x)$ is the transverse beam intensity distribution, β is the thermal and s is the photoexcitation rate. A reduced photoexcitation rate s at infrared wavelengths will result in a smaller amplitude of the space charge field and a smaller refractive index change Δn.

The parameter I_d is usually referred to as 'dark intensity'. Despite its name, I_d depends on light wavelength. The excitation rates are connected with the densities of thermally and photoexcited charge carriers, n_d and n_{ph}, by

$$n = n_d + n_{ph} = \frac{N_D - N_D^+}{\gamma N_D^+} (\beta + s I_b), \tag{3}$$

with γ as the recombination coefficient, and N_D and N_D^+ as the concentration of donors and ionized donors, respectively. The free charge carriers density n is responsible for a conductivity

$$\sigma = \sigma_d + \sigma_{ph}^0 I_b = e\mu(n_d + n_{ph}) = e\mu\left(n_d + \frac{\Phi\tau\alpha}{h\nu} I_b\right). \tag{4}$$

Here σ_d denotes the conductivity in the dark, e the electron charge, and μ the mobility of the charge carriers. The specific photoconductivity σ_{ph}^0 is determined by the photon energy $h\nu$, the quantum efficiency Φ for excitation of a charge carrier, the charge carrier lifetime τ, and the absorption constant α.

By comparison we get the following expression for the wavelength dependence of the dark intensity:

$$I_d(\lambda) = \frac{\beta}{s(\lambda)} = \frac{\sigma_d}{\sigma_{ph}^0(\lambda)} = \frac{n_d hc/\lambda}{\Phi(\lambda)\tau\alpha(\lambda)}, \tag{5}$$

with c as the light velocity.

The space charge field E_{sc} depends on the ratio I_b/I_d. Therefore data are usually referred to

$r := I_b^{max}/I_d$, with I_b^{max} as the maximum value of the beam intensity distribution. The refractive index change caused by the space charge field has to be introduced into the wave equation. Looking for constant soliton solutions, the soliton intensity profile and its width w_0 can be obtained numerically [13], or by analytic approximation [14]. Here the soliton width w_0 for a given intensity ratio r is shown to be solely dependent on a parameter $\xi = k^2 n_e^4 r_{33} E_{ext}$, with $k = 2\pi/\lambda$ [13,14]. The so-called 'existence curves' [15,16] relate the beam width w_0 to the intensity ratio r at a fixed wavelength and external electric field. These curves reveal an absolute minimum of w_0 for $r \approx 1$ and a monotonous increase of the beam width to smaller as well as to larger intensity ratios [17]. Increasing wavelength or decreasing external electric field leads to existence curves with larger beam widths.

3. Experimental

In our experiments we mainly use as-grown, y-cut $Sr_{0.61}Ba_{0.39}Nb_2O_6$ (SBN61), doped with 2000 ppm Rh in the melt. The incorporation coefficient of Rh into SBN61 is well below 1. The crystal dimensions in x, y and z direction are 1.7, 2.5, and 7.8 mm, respectively. Here x is the direction of the ferroelectric c axis and z is the propagation direction of the light beam. Crystals from the same boule with other dimensions, and samples with other dopants (Ce,Cu), are investigated, too. Planar waveguides are fabricated by 2 MeV He^+ implantation at a dose of 10^{15} ions/cm^2 [18], resulting in a barrier waveguide of 5 μm thickness. The implantation dose is deliberately chosen to minimize the influence of the ion-implantation on the photorefractive properties of the waveguiding layer. Rh doping enhances the absorption mainly in the blue–green wavelength region, while in the infrared the absorption is low. The crystal faces perpendicular to the c axis are contacted with silver paste electrodes, by which electric fields up to $E_{ext} = 13$ kV/cm are applied along the direction of the c axis.

We use a standard setup for endface coupling of the light of different lasers into the waveguiding layer [19]. A microscope lens (20× magnification, focal length $f = 9$ mm) focuses the light onto the input face of the waveguide. A second microscope lens (40× magnification) is used to image the light distribution at the endface of the waveguide onto a calibrated IR camera system.

An additional feature of the setup is a cylindrical lens ($f = 300$ mm), acting on the x direction. It is placed in front of the first microscope lens, approximately at a '$2f$' distance (309 mm) to it. Thereby, beams with a nearly constant width along x of about 40 μm throughout the propagation length inside the crystals are produced. This is about twice the expected soliton width, and thus a soliton cannot exist from the input face of the crystal on. Instead, 'tapered' solitons may form after some propagation inside the crystal.

This is not the usual method of producing solitons, so some explanations have to be given. The photorefractive soliton has attractor properties [20], which means, that it can by itself evolve from any intensity distribution that is close enough to the exact soliton profile. Here Gaussian input beams with widths close to the soliton width have been shown to be a good approximation [17,20,21]. Input profiles much wider than the soliton profile are known to split or to show oscillations in width [20,22]. However, we never notice distinct oscillations of the beam width nor an enhanced tendency of the soliton to split. The more common method to produce solitons is to use an input beam which is focused down to the expected soliton width at the input face of the crystal, and which becomes strongly divergent while propagating inside the crystal. In our experiments with infrared light, we were not able to achieve soliton formation with this configuration. By part, we attribute this to the fact that the Gaussian input beam is only an approximation of the soliton profile. Using wider input beams, the beam can reshape itself during propagation by the self-focusing process.

4. Results and discussion

A sufficient large electrooptic coefficient is essential to induce noticeable refractive index changes. We measure the electrooptic coefficient r_{33} for different wavelengths by an interferometric technique [23]. The results are summarized in Fig. 1

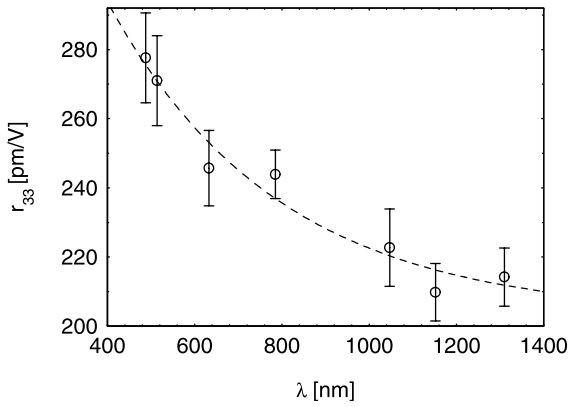

Fig. 1. Electrooptic coefficient r_{33} versus wavelength λ for a bulk SBN crystal doped with 300 ppm Ce. The dashed line is a guide to the eye.

for a slightly doped (300 ppm Ce) bulk crystal. Obviously, the electrooptic coefficient r_{33} is still quite large in the infrared, with a value of 214 pm/V at $\lambda = 1.3$ μm. For ion-implanted waveguides we observe qualitatively the same wavelength dependence. However, the r_{33} values are reduced by factors of 0.9–0.6 in the different waveguide samples, probably due to inhomogeneous poling after implantation.

To investigate the photorefractive self-focusing properties of SBN at telecommunication wavelengths, we first use a DFB laser at $\lambda = 1556$ nm with a power of 2 mW. In Fig. 2 the beam intensity

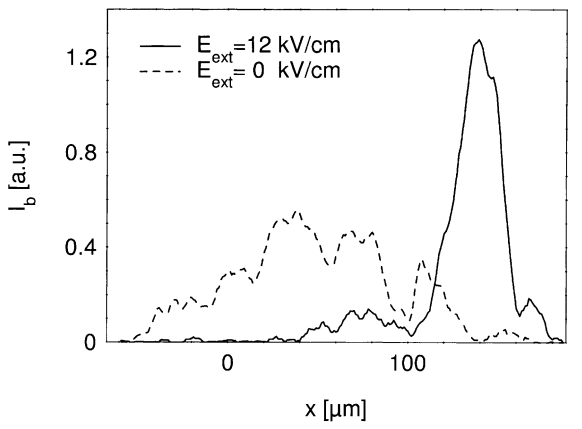

Fig. 2. Intensity distribution I_b at the endface of the waveguide for 2 mW input power at $\lambda = 1556$ nm. (- - -) without external electric field E_{ext}; (—) $E_{ext} = 12$ kV/cm.

distribution I_b versus the x position at the endface of the waveguide is shown, with and without the external field E_{ext} applied. A strong focusing occurs for $E_{ext} = 12$ kV/cm and an intensity at the endface of the waveguide of about 5 W/cm^2. Less pronounced, but distinct photorefractive self-focusing can be observed down to much lower intensities that are at the detection limit of our IR camera. The minimal detectable intensity at $\lambda = 1556$ nm is about 250 μW/cm^2 at the output face of the crystal corresponding to an input laser power of only 100 nW.

To check the influence of the ion implantation, we perform analogous experiments in the bulk of the crystal. The beam focuses as well, however, we do not reach a solitary state. This can be explained from the reduced stability of one-dimensional solitons in three-dimensional media compared to two-dimensional planar waveguides [17,22]. Furthermore, we test self-focusing at $\lambda = 1556$ nm in crystals with other dopants, i.e., 5000 ppm Rh, 300 or 600 ppm Ce, and 500 ppm Cu, and in nominally pure SBN. All other crystals show more or less pronounced self-focusing effects, too. The small influence of the doping is plausible if we assume that its main influence is an absorption enhancement for visible light. At telecommunication wavelengths, however, absorption enhancement is negligible for all these dopants.

Next we investigate the soliton formation process for the 2000 ppm Rh-doped waveguide with a 150 mW laser at $\lambda = 1480$ nm in more detail. In Fig. 3 we illustrate the dependence of the beam width w_0 on the externally applied electric field E_{ext}. The three different input powers, corresponding to beam intensities at the waveguide's endface of about 20, 80, and 300 W/cm^2, represent three different intensity ratios r. For all laser powers, we see strong self-focusing of the light beam for E_{ext} up to 7 kV/cm. At larger external fields E_{ext}, however, the continuous focusing breaks off for the higher input powers 34 and 130 mW. Instead, a nearly constant beam width is reached, which is only slightly decreasing with E_{ext}. This flat part of the w_0 versus E_{ext} curve is the range where solitons are formed, as it is also observed with visible light [19]. The onset of the flat part is dependent on wavelength and intensity, and can be

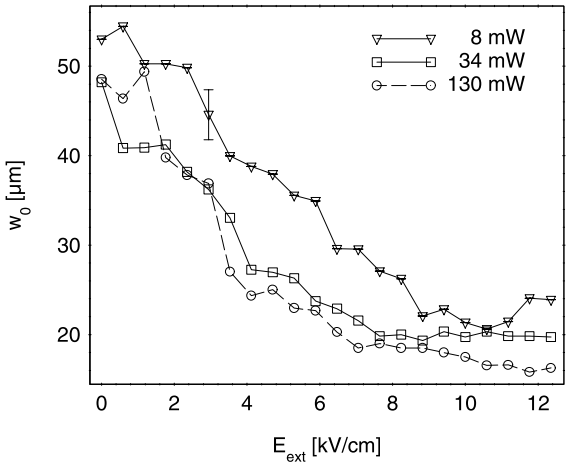

Fig. 3. Beam width w_0 versus external electric field E_{ext} for three different input powers at $\lambda = 1480$ nm (markers). The lines are guides to the eye.

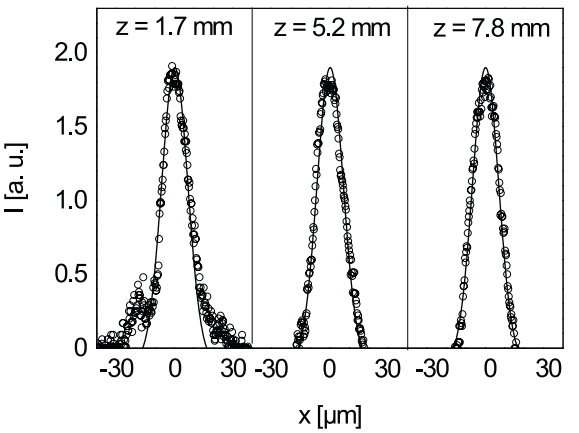

Fig. 4. Beam profiles at the crystal's output face in three 2000 ppm Rh-doped waveguides from the same crystal boule with different lengths $z = 1.7$, 5.2, and 7.8 mm, for $\lambda = 1310$ nm. The input beam width, the intensity at the output faces, and the applied external electric field are $w_0 = 44$ µm, $I_b^{max} = 1050$ W/cm^2, and $E_{ext} = 8$ kV/cm, respectively. The solid Gaussian curve is a guide for the eye.

reached at lower external electric fields if a (slightly) smaller input beam is used.

We verify the soliton existence by checking the output of crystals cut from the same boule, but with different propagation lengths. With the input beam geometry kept constant, we get nearly the same results in the range of external electric fields where solitons are produced. This is shown in Fig. 4, exemplary for the wavelength 1310 nm and an external electric field $E_{ext} = 8$ kV/cm. The beam width at the input faces of the crystals is 44 µm, and this is also the approximate beam width at the endfaces after introducing the three crystals with the lengths $z = 1.7$, 5.2, and 7.8 mm, respectively. The beam intensity, measured at the crystal's output face, is adjusted to $I_b^{max} = 1050$ W/cm^2. While the shape of the output beam at $z = 5.2$ and 7.8 mm is nearly the same, for the 1.7 mm crystal a distinct scattering background is observed. However, the soliton is in principle formed out even after this small propagation length. We usually notice some losses in the convergence from the wider input beam into the soliton, but they in general do not exceed 10%.

As a further confirmation of the soliton formation, we experimentally check the shape of the corresponding existence curve. Here we launch input beams with widths around 40 µm, using again the 1480 nm laser and the 7.8 mm long crystal. An external electric field of 6 kV/cm is sufficient to be in the solitary range. In Fig. 5, the circles mark the beam widths w_0 (FWHM) for different intensities I_b^{max}, measured at the crystal's

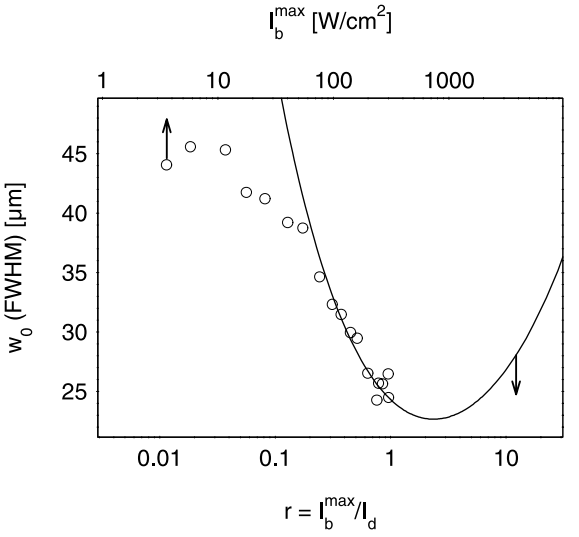

Fig. 5. Beam width w_0 for different intensity ratios r at $\lambda = 1480$ nm. The markers are measured values, and the solid line is the calculated existence curve.

output face. The solid line is the calculated existence curve, i.e., the dependence of w_0 on the intensity ratio $r = I_b^{max}/I_d$, for the parameters of our experiment. Here we use $\lambda = 1480$ nm, $E_{ext} = 6$ kV/cm, $n_e = 2.20$, and $r_{33} = 120$ pm/V. The unknown parameter in superposing the two graphs is the dark intensity I_d at $\lambda = 1480$ nm, which is the scaling factor between the two abscissae. In the ion-implanted waveguides, values of I_d cannot be obtained by conventional conductivity measurements, because the waveguiding layer cannot be isolated from the highly conducting barrier layer and the substrate, respectively. Therefore the comparison of theoretical and measured existence curve provides a useful method to gain information about the important parameter I_d. From Fig. 5, we can deduce the dark intensity $I_d = 300 \pm 70$ W/cm^2 for this waveguide at a wavelength of 1480 nm.

Obviously, with $I_d = 300$ W/cm^2, the experimental data adequately coincide with the theoretical existence curve. A more accurate fit would require higher laser powers to reach the right-hand side of the existence curve. Moreover, at the left-hand side of the existence curve, we observe a deviation from the theoretical curve for r values smaller than 0.1. In part, this might be caused by the use of a narrow input beam in this experiment, which is too small to form the wider solitons. However, even for wider input beams we find that such deviations appear at intensity ratios r of the order of 0.01. Apparently solitons cannot be achieved experimentally for any small intensity I_b. The most probable reason is the use of Gaussian input beams instead of the exact solitary intensity distributions. The Gaussian beam becomes a worse approximation for the soliton profile and the convergence rate from the Gaussian input beam into a solitary regime decreases [24,25] as one moves away from the minimum of the existence curve at $r \approx 1$.

The comparably high value of I_d at $\lambda = 1480$ nm can be explained by the wavelength dependence of the dark intensity. To investigate this, we look at the existence curves at different wavelengths. In the SBN waveguides we can induce solitons and measure existence curves throughout a wavelength range from $\lambda = 0.5$ to 1.5 μm, and

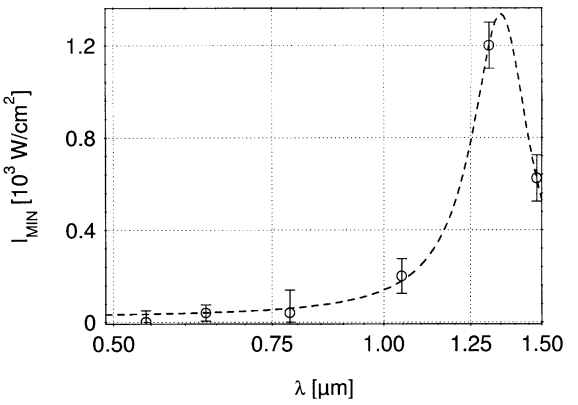

Fig. 6. Beam intensity I_d versus wavelength λ. The dashed line is an exemplary fit.

can compare them to the theoretical curves as shown in Fig. 5. However, it is important to notice that I_d can be estimated even without calculating the exact theoretical curve, since the existence curves attain their minima for a fixed value, i.e., $r = I_b^{max}/I_d \approx 1$. In Fig. 6, we display the beam intensities $I_{MIN} \propto I_d \propto \beta/s$ at the minima of the corresponding existence curves for different wavelengths. The values of I_{MIN} increase from 0.03 W/cm^2 at $\lambda = 543$ nm to 1200 W/cm^2 at $\lambda = 1310$ nm and decrease again for $\lambda = 1480$ nm.

A monotonous increase of the dark intensity with wavelength seems to be most probable when looking at Eq. (5). The origin of the maximum at $\lambda = 1310$ nm is not yet clear. As can be seen from Eq. (5), a maximum of the absorption as well as a minimum of the quantum efficiency near $\lambda = 1.3$ μm is a possible explanation. The infrared absorption of the waveguiding layer is difficult to measure because it can hardly be separated from scattering and tunneling losses. In the bulk material, we measure an absorption which is almost exponentially decaying with wavelength and has no further maximum in the infrared region. However, the introduction of additional absorption bands was sometimes mentioned after ion implantation [9]. On the other hand, the quantum efficiency could have a minimum near 1.3 μm. As an example, the dashed fit in Fig. 6 uses for the quantum efficiency a simple quadratic dependence on wavelength, while the absorption is assumed to be the same as measured in the bulk material.

Additionally, incoherent background illumination is often used to enhance the dark intensity [21]. As Fig. 6 demonstrates, only a strong background illumination, comparable to $I_{MIN} \approx I_d$, can influence the soliton formation at $\lambda = 1310$ nm in our SBN waveguides. Indeed at $\lambda = 1310$ nm a much higher background intensity is needed to influence the solitary intensity distribution than at $\lambda = 1480$ nm.

Finally, the soliton formation times for infrared light are important to be mentioned. The soliton formation time is about 1 s until a steady state is reached, and is thus approximately the same as for visible light [19]. This observation coincides with assumptions based on numerical simulations [26,27].

5. Conclusions

Photorefractive soliton formation should, in principle, be possible for any small refractive index change. A decrease of the refractive index change simply causes a broadening of the soliton. Such a dependence is well known for guided modes and is just what is demonstrated by the form of the existence curves. We thus demonstrate that photorefractive soliton formation is possible even at telecommunication wavelengths around 1.5 μm. Here, SBN61 is shown to be well suited because of a large electrooptic coefficient r_{33} that is still about 200 pm/V in this wavelength region.

The range of beam intensities to induce photorefractive solitons is experimentally limited. In the SBN waveguides, the telecommunication wavelengths are characterized by large values of the so-called 'dark intensity' I_d. Compared to the visible wavelengths region, the beam intensities have to be some orders of magnitude larger to reach the favorable region of intensity ratios $r \approx 1$, i.e., around the minimum of the corresponding existence curve.

The soliton existence curves provide the possibility to measure the wavelength dependence of the dark intensity I_d. In the infrared wavelength region we observe large values of the dark intensity of the order of 10^3 W/cm^2.

While for other photorefractive phenomena, e.g., two-beam coupling, the time constants significantly increase with wavelength, this is not the case for photorefractive solitons. We observe in the infrared soliton formation times of about 1 s until a steady state is reached, which are almost the same as those for visible light.

References

[1] M. Segev, B. Crosignani, A. Yariv, B. Fischer, Phys. Rev. Lett. 68 (1992) 923.
[2] G. Duree, J.L. Schultz, G. Salamo, M. Segev, A. Yariv, B. Crosignani, P. DiPorto, E. Sharp, R.R. Neurgaonkar, Phys. Rev. Lett. 71 (1993) 533.
[3] S. Lan, M. Shih, M. Segev, Opt. Lett. 22 (1997) 1467.
[4] M.D.I. Castillo, P.A.M. Aguilar, J.J. Sanchez-Mondragon, S. Stepanov, V. Vysloukh, Appl. Phys. Lett. 64 (1994) 408.
[5] S. Lan, E. DelRe, Z. Chen, M. Shih, M. Segev, Opt. Lett. 24 (1999) 475.
[6] D. Kip, M. Wesner, C. Herden, V. Shandarov, Appl. Phys. B 68 (1999) 971.
[7] M. Chauvet, S.A. Hawkins, G.J. Salamo, M. Segev, D.B. Bliss, G. Bryant, Appl. Phys. Lett. 70 (1997) 2499.
[8] M. Morin, G. Duree, G. Salamo, M. Segev, Opt. Lett. 20 (1995) 2066.
[9] S. Brülisauer, D. Fluck, P. Günter, L. Beckers, C. Buchal, J. Opt. Soc. Am. B 13 (1996) 2544.
[10] A.W. Snyder, D.J. Mitchell, L. Poladian, F. Ladouceur, Opt. Lett. 16 (1991) 21.
[11] K. Buse, U. van Stevendaal, R. Pankrath, E. Krätzig, J. Opt. Soc. Am. B 13 (1996) 1461.
[12] M.I. Carvalho, S.R. Singh, D.N. Christodoulides, Opt. Commun. 120 (1995) 311.
[13] D.N. Christodoulides, M.I. Carvalho, J. Opt. Soc. Am. B 12 (1995) 1628.
[14] G. Montemezzani, P. Günter, Opt. Lett. 22 (1997) 451.
[15] M. Segev, G.C. Valley, B. Crosignani, P. DiPorto, A. Yariv, Phys. Rev. Lett. 73 (1994) 3211.
[16] M. Segev, M. Shih, G. Valley, J. Opt. Soc. Am. B 13 (1996) 706.
[17] K. Kos, H. Meng, G. Salamo, Phys. Rev. E 53 (1996) R4330.
[18] D. Kip, B. Kemper, I. Nee, R. Pankrath, P. Moretti, Appl. Phys. B 65 (1997) 511.
[19] D. Kip, M. Wesner, V.M. Shandarov, P. Moretti, Opt. Lett. 23 (1998) 921.
[20] A.A. Zozulya, D.Z. Anderson, Phys. Rev. A 57 (1998) 552.
[21] M.F. Shih, P. Leach, M. Segev, M.H. Garrett, G. Salamo, G.C. Valley,, Opt. Lett. 21 (1996) 324.
[22] A.V. Mamaev, M. Saffman, D.Z. Anderson, A.A. Zozulya, Phys. Rev. A 54 (1996) 870.
[23] K. Onuki, N. Uchida, T. Saku, J. Opt. Soc. Am. 62 (1972) 1030.

[24] R. Ryf, M. Wiki, G. Montemezzani, P. Günter, A.A. Zozulya, Opt. Commun. 159 (1999) 339.
[25] A.A. Zozulya, D.Z. Anderson, A.V. Mamaev, M. Saffman, Europhys. Lett. 36 (1996) 419.
[26] N. Fressengeas, D. Wolfersberger, J. Maufoy, G. Kugel, J. Korean Phys. Soc. 32 (1998) 414 1998.
[27] N. Fressengeas, D. Wolfersberger, J. Maufoy, G. Kugel, Opt. Commun. 32 (1998) 414.